https://doi.org/10.46861/bmp.32.105 PŮVODNÍ PRÁCE/ORIGINAL PAPER

Bismuth phosphates from the Sítio do Castelo mine, Folgosinho (Portugal): description and Raman spectroscopy

Jaromír Tvrdý[1)], Luboš Vrtiška[1)]*, Jiří Sejkora[1)], Pierre Rosseel[2)] a Zdeněk Dolníček[1)]

[1)]*Department of Mineralogy and Petrology, National Museum, Cirkusová 1740, CZ-19300 Praha 9 - Horní Počernice, Czech Republic; *e-mail: lubos.vrtiska@nm.cz*
[2)]*Nazaret dreef 103, B-2500 Lier, Belgium*

Tvrdý J, Vrtiška L, Sejkora J, Rosseel P, Dolníček Z (2024) Bismuth phosphates from the Sítio do Castelo mine, Folgosinho (Portugal): description and Raman spectroscopy. Bull Mineral Petrolog 32(2): 105-113 ISSN 2570-7337

Abstract

Two bismuth phosphates, zaïrite and monoclinic analogue of ximengite, are described from the Sítio do Castelo mine, Folgosinho (Portugal). Zaïrite is known from Folgosinho for a long time, but no analytical data have been published so far. On the studied samples, it forms bright yellow crystals of variable morphology, from tabular to columnar and spindle-shaped crystals. Electron microprobe analysis showed the relative purity of the zaïrite with a minor content of elements typical for minerals of the plumbogummite group. The empirical formula can be expressed as $(Bi_{0.84}Sr_{0.08}Ca_{0.06}Pb_{0.01})_{\Sigma 0.99}Fe_{3.07}[(PO_4)_{1.91}(SO_4)_{0.09}]_{\Sigma 2.00}[(OH)_{6.01}F_{0.09}]_{\Sigma 6.10}$. The Raman spectrum of zaïrite is dominated by vibrational bands of $(PO_4)^{3-}$ and $(OH)^-$ units. Monoclinic bismuth orthophosphate, unknown as a mineral species until now, was rarely found as aggregate up to 30 μm in size rimmed by zaïrite. Its empirical formula is $(Bi_{0.97}Fe_{0.04}Ca_{0.02})_{\Sigma 1.02}(PO_4)_{1.00}F_{0.09}$. The Raman spectrum agrees with published data for the $BiPO_4$ polymorph of $SbPO_4$-type, space group $P2_1/m$. The two described bismuth phosphates at the Sítio do Castelo mine were formed by the decomposition of unspecified primary bismuth minerals due to the activity of late hydrothermal to supergene phosphorus-rich solutions.

Key words: *zaïrite, plumbogummite group, $BiPO_4$, monoclinic analogue of ximengite, chemical composition, Raman spectroscopy, Folgosinho, Portugal*

Received 3. 10. 2024; accepted 28. 11. 2024

Introduction

Chemical compounds based on bismuth have recently been intensively investigated for their applicability as photocatalysts for energy conversion and environmental applications, in particular decomposition of organic pollutants and their further mineralization to CO_2 and H_2O (e.g. Wang et al. 2013; Di et al. 2017; Pan, Zhu 2015; Naciri et al. 2020; Monteles et al. 2023). Bismuth phosphates are used also as ion and humidity sensors, microwave dielectric, host for luminescent ions and for the separation and immobilization of radioactive elements (Errandonea et al. 2015). In nature, phosphates containing bismuth in their chemical formula are relatively rare minerals, representing only a dozen of the more than six thousand valid species included in the List of Minerals recognized by the Commission on New Minerals, Nomenclature and Classification of the International Mineralogical Association as of September 2024. Two of these phases - zaïrite and monoclinic analogue of ximengite - were identified during the study of secondary mineral assemblages from the Sítio do Castelo mine, Folgosinho (Portugal).

The mineral zaïrite, first described by Van Wambeke (1975) in a weathering zone of tungsten-rich quartz veins in Eta-Etu, North Kivu, DR Congo (Zaire), is reported from only a few occurrences worldwide (Mindat 2024b). From Folgosinho, it is known for a longer time, but no analytical data were published so far (Alves et al. 2016).

Another bismuth phosphate occurring with zaïrite on samples from Eta-Etu is hexagonal $BiPO_4$ described later by Shi (1989a, 1989b) under the name ximengite (Jambor, Vanko 1991). In addition to the original occurrence at the Amo tin deposit, Ximen County, Yunnan (China), ximengite is reported from several other localities (Mindat 2024a), but because of the small grain size often only on the basis of microprobe analyses and without confirmation of which $BiPO_4$ modification it actually represents. This is also the case for the occurrence in altered sulphotellurides from the Limarinho gold deposit in Portugal (Cepedal et al. 2013). The Folgosinho find published here is the first confirmed discovery of monoclinic anhydrous bismuth phosphate formed in natural conditions.

Occurrence

The Sítio do Castelo mine is located east of the medieval Folgosinho village in the Serra da Estrela National Park in central Portugal (GPS 40.511389° N, 7.508056° W). The first mining works date back to 1917 when tin-tungsten ores in short galleries were mined. Between 1976 and 1986, quartz raw material was exploited for the production of metallic silicon in a small wall quarry (Alves et al. 2016). The ore mineralization was followed by extending upslope above the quarry level. The main quartz body is about 5 m thick and steeply penetrates migmatitised schists. It is considered to be either the core of a large pegmatite (pers. comm. A. Lima 2021) or a high-temperature hydrothermal vein accompanied by greisenisation of surrounding rocks (Garate-Olabe et al. 2012).

Fig. 1 *Clear yellow zaïrite crystal on pinkish phosphosiderite. FOV 1 mm. Photo by L. Vrtiška.*

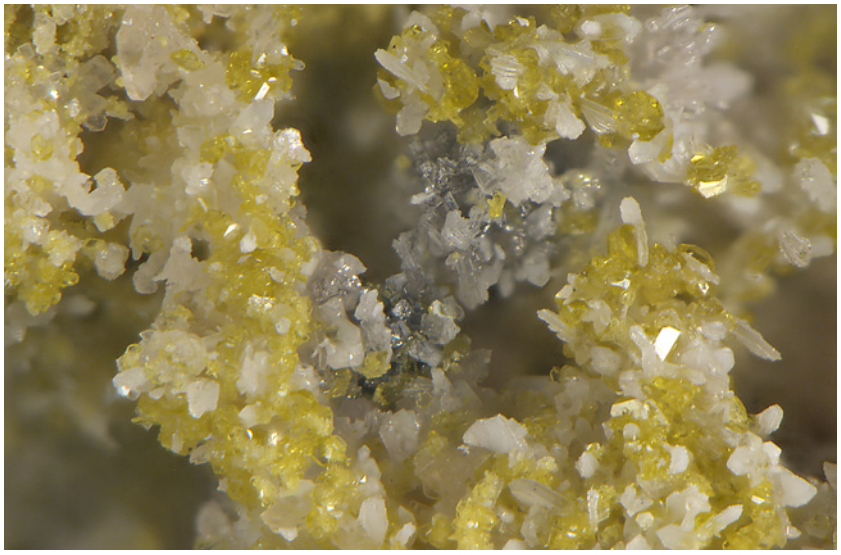

Fig. 2 *Bright yellow zaïrite with pale phosphosiderite/strengite. FOV 1.4 mm. Photo by L. Vrtiška.*

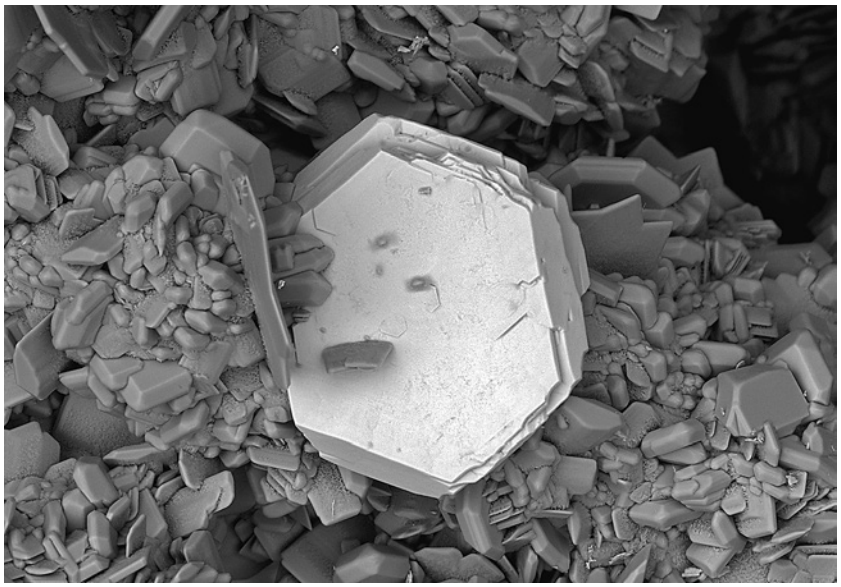

Fig. 3 *Flattened zaïrite crystal on phosphosiderite. FOV 320 μm. SEM-BSE photo by B. Ekrt.*

Irregular phosphate accumulations and sulphide aggregates (pyrite >> arsenopyrite >> chalcopyrite >> sphalerite) occur frequently in the main body. Primary phosphates are represented predominantly by zwieselite-triplite and less commonly by isokite with admixed fluorapatite. Intense weathering yielded varied secondary phosphate assemblages, which differ concerning their source mineral. While phosphosiderite, strengite, rockbridgeite-frondelite, cacoxenite, bermanite, beraunite, strunzite, stewartite, laueite, leucophosphite, benyacarite, fluorapatite, wavellite and kidwellite are related to the alteration of zwieselite-triplite, products resulting from triplite-zwieselite in association with fluorapatite and isokite include ludlamite, vivianite, strunzite-zincostrunzite, Zn-rich rockbridgeite-frondelite, Mn-rich phosphophyllite, hydroxylapatite, jahnsite-(CaMnFe), earlshannonite, lun'okite, plimerite and ferraioloite (Alves et al. 2016; Kampf et al. 2017; Tvrdý et al. 2021).

In addition to these associations, occurrences of mineral compounds containing other, less common chemical elements are known. One of these elements is bismuth, which is the main constituent of two minerals described here, zaïrite and a monoclinic analogue of ximengite, both found in the cavities of altered quartz veins with relics of sulphide Bi-mineralisation in the peripheral parts of the main body.

The studied samples with bismuth phosphates from Folgosinho are kept in the Mineralogical Collection of the National Museum in Prague under the inventory number P1N118285 (5 fragments).

Methods

Colour microphotographs were taken using a Nikon SMZ25 microscope with a Nikon DS-Ri2 digital camera and the image assembling function using NIS Elements AR version 4.20. Photographs of zaïrite in back-scattered electrons were taken on a Hitachi S3700-N scanning electron microscope at a voltage of 15 kV (Boris Ekrt, National Museum, Prague).

Samples were analysed with a Cameca SX-100 electron microprobe (National Museum, Prague) operating in the wavelength-dispersive mode with an accelerating voltage of 15 kV, a specimen current of 10 nA, and a beam diameter of

2 μm. The following lines and standards were used: apatite (P*K*α, Ca*K*α), celestite (S*K*α, Sr*L*β), hematite (Fe*K*α), LiF (F*K*α), vanadinite (Pb*M*α), Bi (Bi*M*α). Peak counting times (CT) were 20 s; CT for each background was one-half of the peak time. The raw intensities were converted to the concentrations automatically the using *PAP* (Pouchou, Pichoir 1985) matrix-correction procedure. The contents of As, Na, Al, Mg, Si, Cl, K, Mn, Cu, Zn, N, V and Cr were also sought but always found to be below the detection limits (about 0.05 - 0.20 wt.%). Water content could not be analysed directly because of the minute amount of material available.

The Raman spectra were collected in the range 4200 - 40 cm^{-1} using a DXR dispersive Raman Spectrometer (Thermo Scientific) mounted on a confocal Olympus microscope. The Raman signal was excited by an unpolarized 532 nm diode-pumped solid-state laser and detected by a CCD detector. The experimental parameters were: 50× objective, 6 s exposure time, 300 exposures, 50 μm pinhole spectrograph aperture and 4 mW laser power level (zaïrite) and 100× objective, 1 s exposure time, 90 exposures, 50 μm pinhole spectrograph aperture and 10 mW laser power level (monoclinic $BiPO_4$). The spectra were repeatedly acquired from different grains in order to obtain a representative spectrum with the best signal-to-noise ratio. The eventual thermal damage of the measured point was excluded by visual inspection of excited surface after measurement, by observation of possible decay of spectral features in the start of excitation and checking for thermal downshift of Raman lines. The instrument was set up by a software-controlled calibration procedure using multiple neon emission lines (wavelength calibration), multiple polystyrene Raman bands (laser frequency calibration) and standardized white-light sources (intensity calibration). Spectral manipulations were performed using the Omnic 9 software (Thermo Scientific). Gaussian/Lorentzian (pseudo-Voigt) profile functions of the band-shape were used to obtain decomposed band components of the spectra. The decomposition was based on the minimization of the difference in the observed and calculated profiles until the squared correlation coefficient (r^2) was greater than 0.995.

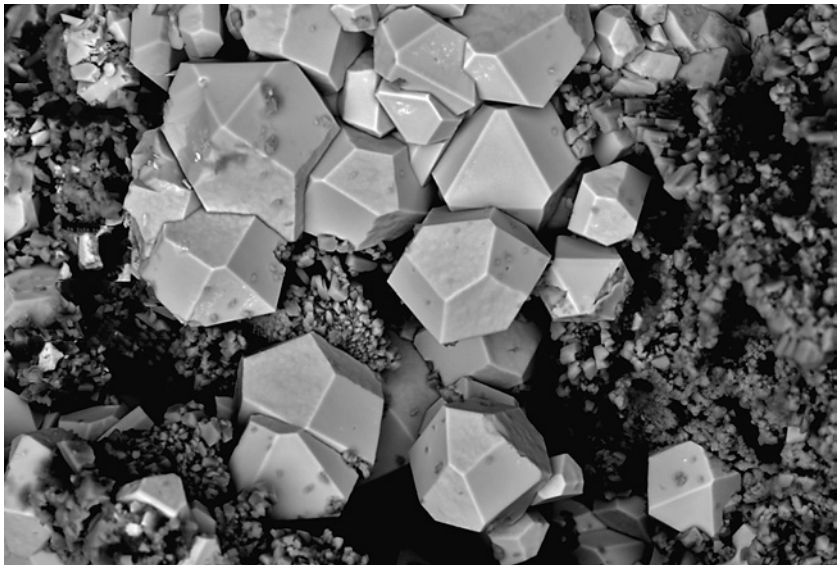

Fig. 4 *Isometric trigonal zaïrite crystals. FOV 130 μm. SEM-BSE photo by B. Ekrt.*

Fig. 5 *Clusters of columnar zaïrite crystals. FOV 160 μm. SEM-BSE photo by B. Ekrt.*

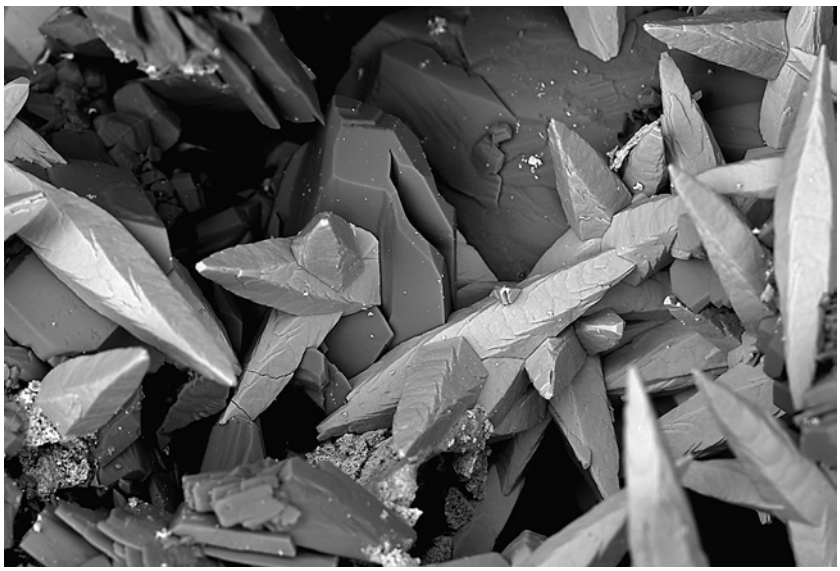

Fig. 6 *Spindle-shaped scalenohedral crystals of zaïrite. FOV 250 μm. SEM--BSE photo by B. Ekrt.*

Results

Zaïrite

Despite its very small size, zaïrite is easily visible due to its bright yellow colour and glassy to diamond-like lustre. It most commonly grows on crystalline aggregates of pale phosphosiderite and/or strengite (Fig. 1, Fig.2). According to the dominance of one of the main crystal shapes (pinacoid, rhombohedron, scalenohedron), four morphological types of zaïrite were observed on different samples: (a) pseudohexagonal plates with pinacoid dominance (Fig. 3), (ii) almost isometric crystals (Fig. 4), (iii) elongated columnar crystals (Fig. 5), and (iv) spindle-shaped and sharply pointed scalenohedra (Fig. 6).

Results of the chemical analysis of zaïrite from Folgosinho are given in Table 1. The cation site is dominated by Bi (0.75 - 0.93 *apfu*), with minor contents of Sr (0.02 - 0.13 *apfu*), Ca (0.01 - 0.09 *apfu*) and Pb (0.00 - 0.02 *apfu*) showing assignment to the plumbogummite group. In the anionic site, minor S (0.03 - 0.15 *apfu*) is present in addition to the dominant P (1.86 - 1.97 *apfu*). The fluorine replacing the hydroxyl group is also low (0.00 - 0.19 *apfu*). Neither Al, present in 22% of the Fe site of the original zaïrite (Van Wambeke 1975), nor the As reported by Alves et al. (2016) were detected in the younger generation of zaïrite from Folgosinho. The empirical formula of the mineral on the basis of P+S = 2 *apfu* (average of 13 analyses) can be expressed as $(Bi_{0.84}Sr_{0.08}Ca_{0.06}Pb_{0.01})_{\Sigma 0.99}Fe_{3.07}[(PO_4)_{1.91}(SO_3)_{0.09}]_{\Sigma 2.00}[(OH)_{6.01}F_{0.09}]_{\Sigma 6.10}$.

Crystal structural data for zaïrite were not published so far, but it is assumed that the mineral has a similar structure to its Al-analogue waylandite, as described by Mills et al. (2010). In the asymmetric part of the trigonal (space group *R*-3*m*, *Z* = 3) waylandite unit-cell (Mills et al.

Table 1 *Chemical composition of zaïrite from Folgosinho (wt.%)*

	Mean	1	2	3	4	5	6	7	8	9	10	11	12	13
CaO	0.47	0.42	0.32	0.43	0.09	0.75	0.79	0.68	0.79	0.71	0.27	0.13	0.58	0.15
SrO	1.26	0.58	0.28	1.28	0.80	1.81	1.77	2.03	1.42	1.84	1.28	0.94	1.53	0.83
PbO	0.37	0.00	0.00	0.39	0.36	0.40	0.51	0.63	0.48	0.68	0.29	0.36	0.33	0.37
Bi_2O_3	29.57	31.16	32.38	30.56	30.82	28.09	27.90	27.46	28.01	27.98	29.81	30.72	29.38	30.09
Fe_2O_3	37.02	35.31	36.26	37.36	37.16	37.72	37.86	38.36	37.67	37.57	37.23	37.32	35.83	35.55
P_2O_5	20.48	20.15	20.80	20.07	20.58	20.05	20.52	20.65	20.65	20.14	20.35	21.18	20.36	20.79
SO_3	1.10	0.69	0.36	1.24	0.58	1.77	1.73	1.77	1.45	1.58	1.11	0.33	1.31	0.36
F	0.25	0.30	0.25	0.29	0.53	0.00	0.23	0.00	0.21	0.16	0.35	0.47	0.00	0.52
H_2O*	8.19	7.83	8.06	8.52	8.13	8.58	8.34	8.53	8.26	8.46	8.23	8.07	8.42	8.08
O=F	-0.11	-0.13	-0.11	-0.12	-0.22	0.00	-0.10	0.00	-0.09	-0.07	-0.15	-0.20	0.00	-0.22
Total	98.60	96.31	98.60	100.02	98.83	99.17	99.55	100.11	98.85	99.06	98.77	99.32	97.74	96.52
Ca	0.055	0.051	0.038	0.051	0.011	0.088	0.091	0.077	0.091	0.083	0.032	0.015	0.068	0.018
Sr	0.080	0.038	0.018	0.083	0.052	0.115	0.110	0.125	0.089	0.117	0.082	0.060	0.097	0.054
Pb	0.011	0.000	0.000	0.012	0.011	0.012	0.015	0.018	0.014	0.020	0.009	0.011	0.010	0.011
Bi	0.839	0.914	0.934	0.880	0.890	0.792	0.771	0.753	0.778	0.791	0.851	0.872	0.832	0.868
Σ	0.986	1.004	0.991	1.025	0.964	1.006	0.986	0.974	0.972	1.012	0.974	0.958	1.007	0.951
Fe	3.067	3.023	3.052	3.137	3.132	3.102	3.052	3.069	3.053	3.101	3.102	3.090	2.960	2.994
PO_4	1.909	1.941	1.970	1.896	1.951	1.855	1.861	1.859	1.880	1.870	1.908	1.973	1.725	1.754
PO_3OH	0.000	0.000	0.000	0.000	0.000	0.000	0.000	0.000	0.003	0.000	0.000	0.000	0.167	0.216
SO_3	0.091	0.059	0.030	0.104	0.049	0.145	0.139	0.141	0.117	0.130	0.092	0.027	0.108	0.030
Σ	2.000	2.000	2.000	2.000	2.000	2.000	2.000	2.000	2.000	2.000	2.000	2.000	2.000	2.000
F	0.089	0.108	0.088	0.102	0.188	0.000	0.078	0.000	0.072	0.055	0.123	0.164	0.000	0.184
OH	6.014	5.943	6.014	6.344	6.074	6.254	5.960	6.049	5.928	6.192	6.076	5.920	6.000	5.816
Σ	6.103	6.051	6.102	6.447	6.262	6.254	6.038	6.049	6.000	6.247	6.199	6.083	6.000	6.000

Mean of 13 point analyses; *apfu* on the base P+S = 2; H_2O* contents were calculated on the basis of charge balance.

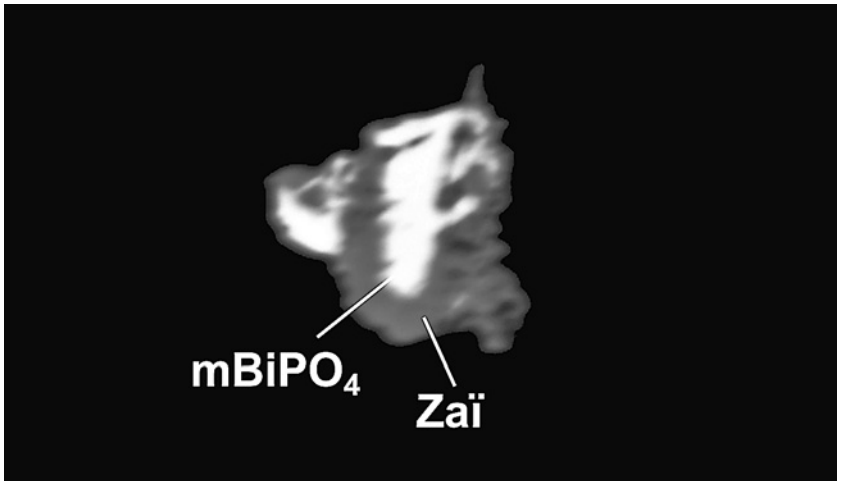

Fig. 7 *Monoclinic analogue of ximengite (white) overgrown with zaïrite (grey). FOV 150 µm. BSE photo by Z. Dolníček.*

2010), there are one symmetrically distinct Bi, one Al, one $(PO_4)^{3-}$ and one $(OH)^-$ unit. Waylandite has an alunite-type structure comprised of a rhombohedral stacking of (001) composite layers of corner-shared AlO_6 octahedra and PO_4 tetrahedra, with Bi atoms occupying icosahedrally coordinated sites between the layers (Mills et al. 2010).

The full-range Raman spectrum of the studied zaïrite is given in Figure 8; Raman spectrum of this mineral has not been published yet and is not even included in the RRUFF database (Lafuente et al. 2015). Tentative interpretation of spectrum (Table 2) is based on papers of Nakamoto (2009), Frost et al. (2013) and Tvrdý et al. (2021). A broad intensive band with components at 3356, 3109 and 2944 cm^{-1} (Fig. 9a) is connected with ν OH stretching vibrations of hydrogen-bonded hydroxyls $(OH)^-$. According to Libowitzky (1999), approximate O-H···O hydrogen bond lengths vary in the range from 2.77 to 2.64 Å. These lengths are comparable with a weak hydrogen bond 2.77 Å found in the crystal structure of waylandite (Mills et al. 2010). The medium intensity bands in the region 1200 - 800 cm^{-1} (Fig. 9b) are assigned to dominant stretching vibrations of $(PO_4)^{3-}$ groups; bands at 1179, 1122, 1084 and 1034 cm^{-1} to the ν_3 triply degenerate antisymmetric stretching vibrations and those at 1010, 990 and 912 cm^{-1} to the ν_1 symmetric stretching vibrations, respectively. The presence of stretching vibrations of minor components of studied mineral - $(SO_4)^{2-}$ (usually 1100 - 980 cm^{-1}, e.g. Nakamoto 2009; Sejkora et al. 2023) and $(PO_3OH)^{2-}$ groups (1170 - 940 cm^{-1}, e.g. Pechkovski et al. 1981; Frost et al. 2013) in this region cannot be excluded. Bands at 625, 599, 572 and 551 cm^{-1} (Fig. 9c) are assigned to the split triply degenerate ν_4 (δ) $(PO_4)^{3-}$ out-of-plane bending vibrations and those at 474, 457, 438 and 411 cm^{-1} to the doubly degenerate ν_2 (δ) $(PO_4)^{3-}$ out-of-plane bending vibration. The Fe-O stretching and O-Fe-O bending vibrations of FeO_6 octahedra are related to bands observed at 378, 297, 240, 221 and 202 cm^{-1} (Fig. 9d). Bands at 163, 115, 97 and 58 cm^{-1} (Fig. 9d) are attributed to lattice modes.

Monoclinic $BiPO_4$

The monoclinic analogue of ximengite has not been visually observed and was discovered only in the polished section by electron microprobe. It was found in a single case as an irregular grain of about 30 μm overgrown with zaïrite (Fig. 7). Chemical analysis given in Table 3 shows low Fe (0.03 - 0.04 *apfu*) and Ca (0.02 *apfu*) contents replacing Bi (0.95 - 0.99 *apfu*) in the structure. The presence of fluorine (0.09 - 0.11 *apfu*) was detected, which could indicate a weak hydroxylation of the mineral. The empirical formula (average of 6 analyses) is $(Bi_{0.97}Fe_{0.04}Ca_{0.02})_{\Sigma 1.02}(PO_4)_{1.00}F_{0.09}$.

Crystal structures, thermal behavior, IR and Raman data for three known polymorphs of $BiPO_4$ were published

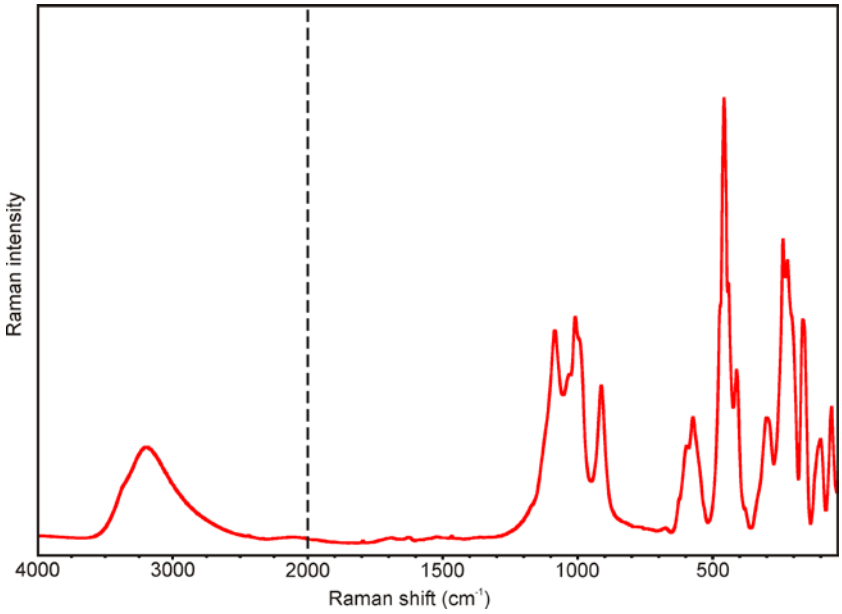

Fig. 8 *Raman spectrum of zaïrite from Folgosinho (split at 2000 cm^{-1}).*

Table 2 *Tentative assignment of Raman spectrum of zaïrite from Folgosinho*

Position [cm^{-1}]	FWHH [cm^{-1}]	I_{rel}^H [%]	$I_{rel.}^A$ [%]	Tentative assignment
3356	129	4.2	10.4	ν OH stretch of hydroxyls (OH)
3190	262	20.2	100.0	
2944	240	6.7	32.2	
1179	52	3.6	4.4	ν_3 $(PO_4)^{3-}$ antisymmetric stretch
1122	48	15.2	17.3	
1084	42	43.4	44.5	
1034	53	30.8	39.0	
1010	16	20.1	7.4	ν_1 $(PO_4)^{3-}$ symmetric stretch
990	34	39.4	34.9	
912	34	35.4	30.9	
625	15	4.4	1.5	ν_4 (δ) $(PO_4)^{3-}$ out-of-plane bend
599	30	19.3	13.2	
572	26	24.5	14.4	
551	27	12.9	7.9	
474	21	39.8	20.4	ν_2 (δ) $(PO_4)^{3-}$ out-of-plane bend
457	18	100.0	39.8	
438	19	44.7	21.0	
411	23	38.6	20.8	
378	14	3.4	1.1	Fe-O stretch and O-Fe-O symmetric band
297	56	32.3	45.7	
240	25	65.0	39.7	
221	19	45.3	20.2	
202	24	47.0	24.1	
163	22	58.4	24.8	lattice modes
115	22	20.4	10.2	
97	20	24.7	11.1	
58	28	39.9	26.6	

$I_{rel.}$ calculated from the band height (^{H}) and band area (^{A}).

in several papers (e.g. Wang et al. 2013; Achary et al. 2013; Monteles et al. 2023; Haq et al. 2024). Achary et al. (2013) refers to these modifications as a trigonal Phase I (space group $P3_121$; HBIP of Pan, Zhu 2015) corresponding to mineral ximengite (Shi 1989a, 1989b) and monoclinic Phase II (monazite-type, space group $P2_1/n$; nMBIP of Pan, Zhu 2015) and Phase III ($SbPO_4$-type, space group $P2_1/m$; mMBIP of Pan, Zhu 2015).

The Raman spectrum of the studied $BiPO_4$ from Folgosinho agrees with data for Phase III published by Achary et al. (2013) and is distinctly different from the spectra of both other polymorphic modifications of $BiPO_4$. The Phase III of Achary et al. (2013) is monoclinic, space group $P2_1/m$, $SbPO_4$-type, with unit-cell parameters a 4.8807(2), b 7.0674(3), c 4.7023(2) Å, β 96.303(4)°, V 161.22 Å^3 and Z = 4. This phase is referred to as high-temperature and was synthesized at a temperature of 973 K; concurrently it is stable in the temperature range 300 - 1173 K and it is the most thermodynamically stable modification of $BiPO_4$ (Achary et al. 2013). According to Wang et al. (2013), the structural framework consists of the building blocks of PO_4 tetrahedra and BiO_8 polyhedra. Each BiO_8 poly-

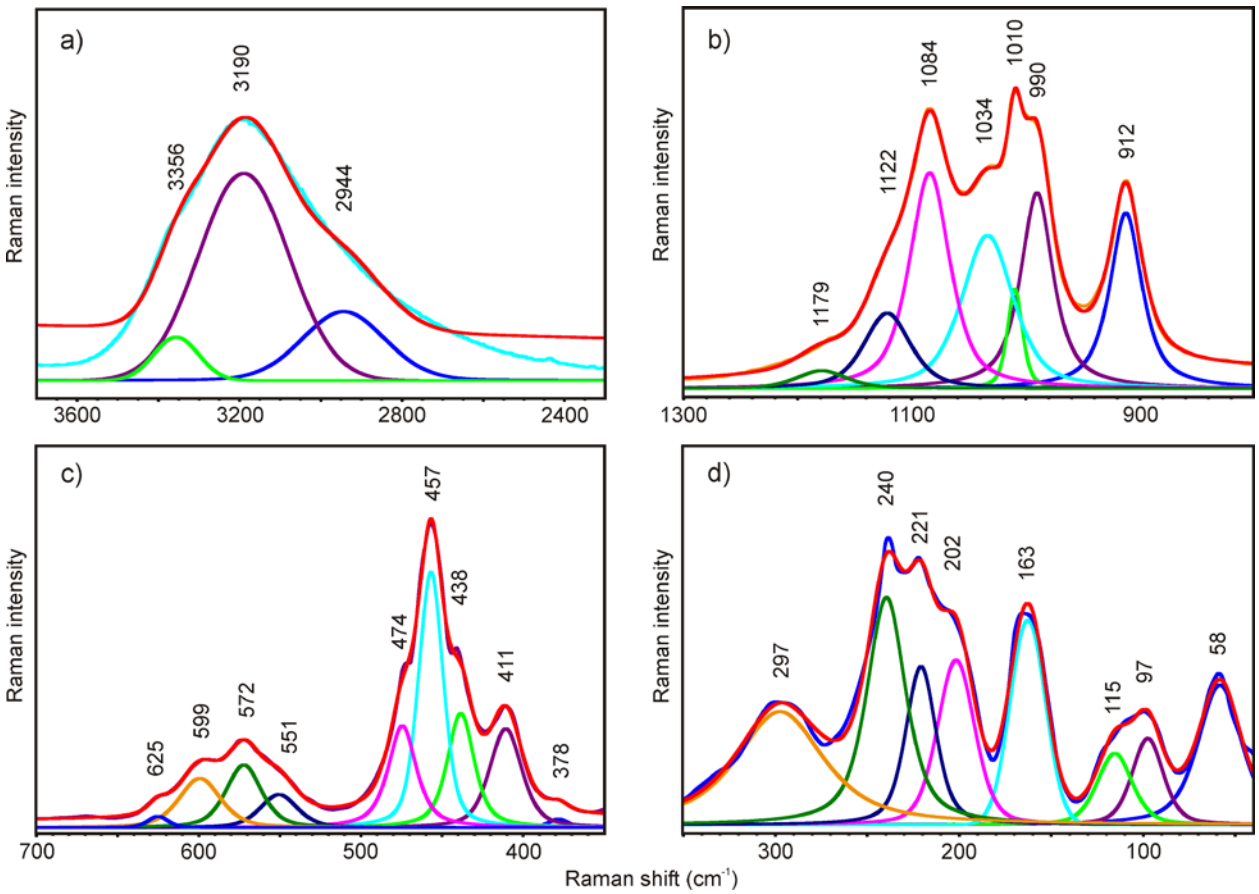

Fig. 9 *Results of the band component analysis of the Raman spectrum of zaïrite from Folgosinho: a) 3700 - 2300 cm^{-1}; b) 1300 - 800 cm^{-1}; c) 700 - 350 cm^{-1}; d) 350 - 40 cm^{-1}.*

Table 3 *Chemical composition of monoclinic analogue of ximengite from Folgosinho (wt.%)*

	Mean	1	2	3	4	5	6
Bi_2O_3	73.23	73.06	73.56	72.95	72.73	73.68	73.42
Fe_2O_3	0.90	1.08	0.84	0.89	0.87	0.91	0.82
CaO	0.32	0.32	0.33	0.32	0.31	0.31	0.32
P_2O_5	23.02	22.97	22.73	23.03	23.19	22.69	23.48
F	0.58	0.66	0.52	0.59	0.62	0.52	0.55
F=O	-0.24	-0.28	-0.22	-0.25	-0.26	-0.22	-0.23
Total	97.80	97.81	97.76	97.53	97.46	97.89	98.36
Bi	0.969	0.967	0.984	0.965	0.955	0.989	0.953
Fe	0.035	0.042	0.033	0.034	0.033	0.036	0.031
Ca	0.018	0.018	0.018	0.018	0.017	0.017	0.017
Σ	1.022	1.027	1.035	1.017	1.005	1.042	1.001
P	1.000	1.000	1.000	1.000	1.000	1.000	1.000
F	0.094	0.107	0.085	0.096	0.100	0.086	0.088

Mean of 6 point analyses; *apfu* on the base P = 1.

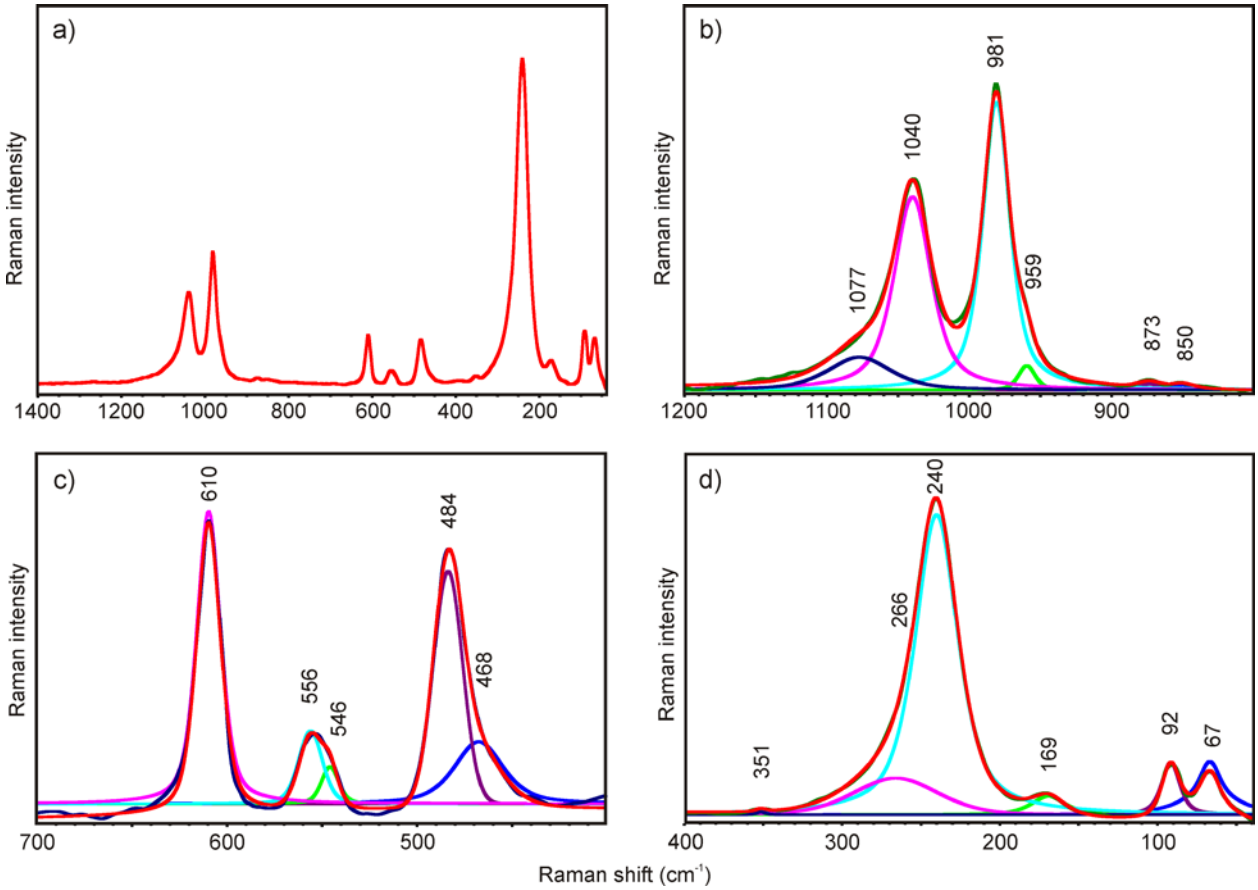

Fig. 10 *a) Raman spectrum for monoclinic $BiPO_4$ from Folgosinho and results of the band component analysis: b) 1200 - 800 cm^{-1}; c) 700 - 400 cm^{-1}; d) 400 - 40 cm^{-1}.*

Table 4 *Tentative assignment of Raman spectra of monoclinic $BiPO_4$ from Folgosinho*

Folgosinho				$BiPO_4$*		
Position [cm^{-1}]	FWHH [cm^{-1}]	I_{rel}^{H} [%]	$I_{rel.}^{A}$ [%]	Position [cm^{-1}]	$I_{rel.}$	Tentative assignment
1077	52	4.5	7.0	1046	m	ν_3 $(PO_4)^{3-}$ antisymmetric stretch
1040	31	26.8	25.7	1038	m	
981	23	40.0	28.7	982	m	ν_1 $(PO_4)^{3-}$ symmetric stretch
959	14	3.4	1.4	966	m	
873	18	0.8	0.4			
850	20	0.7	0.4			
610	15	15.9	6.9	610	m	
556	15	4.0	1.5	558	w	ν_4 (δ) $(PO_4)^{3-}$ out-of-plane-bend
546	11	2.0	0.6	548	m	
484	18	12.6	5.4	486	m	ν_2 (δ) $(PO_4)^{3-}$ in-plane bend
468	30	3.4	3.0			
351	7	0.9	0.2	354	w	
266	63	12.2	20.0			
240	32	100.0	100.0	244	vs	internal modes of BiO_8 polyhedra
				214	w	
169	25	6.2	4.9	179	m	
				145	vw	
				130	vw	
92	13	17.4	7.2	92	m	lattice modes
67	20	17.7	13.6	69	vs	
				56	w	

$BiPO_4$* - data published by Achary et al. (2013) for synthetic monoclinic $BiPO_4$ - III ($SbPO_4$ - Type); $I_{rel.}$ calculated from the band height (^{H}) and band area (^{A}).

hedron is connected to the other one by sharing the edge, and each PO_4 tetrahedron is coordinated to six BiO_8 polyhedra, in which two are connected by edge and other four are shared by the top.

The distinct bands were observed in the Raman spectrum of monoclinic analogue of ximengite from Folgosinho in the region 1400 - 400 cm^{-1} (Fig. 10a). Tentative interpretation of spectrum (Table 4) is based on papers of Nakamoto (2009) and Achary et al. (2013). A medium--intensity band with two components at 1077 and 1040 cm^{-1} (Fig.10b) is assigned to the split triply degenerate ν_3 $(PO_4)^{3-}$ antisymmetric stretching vibrations. A band at 981 cm^{-1} with shoulder at 959 cm^{-1} (Fig. 10b) is attributed to the ν_1 $(PO_4)^{3-}$ symmetric stretching vibrations. Bands at 610, 556 and 546 cm^{-1} (Fig. 10c) are assigned to the split triply degenerate ν_4 $(PO_4)^{3-}$ out-of-plane bending vibrations. A band at 484 cm^{-1} with shoulder at 468 cm^{-1} (Fig. 10c) relates to the split doubly degenerate ν_2 $(PO_4)^{3-}$ in--plane bending vibrations. A strong band at 240 cm^{-1} with shoulder at 266 cm^{-1} and a weak band at 169 cm^{-1} (Fig. 10d) are attributed to internal vibrational modes of BiO_8 polyhedra (Achary et al. 2013). Very weak bands at 873, 850 and 351 cm^{-1} may be assigned to overtones, bands at 92 and 67 cm^{-1} are attributed to lattice modes.

Discussion

The obvious sources of bismuth at the Folgosinho site are Bi-sulphides or native bismuth, which are characteristic admixtures in quartz veins as well as pegmatites. The described phosphates were formed due to the activity of late hydrothermal to supergene fluids with high phosphorus content and its rarity reflects the rarity of primary bismuth minerals at the locality. The monoclinic $BiPO_4$ is apparently older, probably formed by direct replacement of primary minerals at higher temperatures. This can be inferred from the data on the synthesis temperatures of the individual modifications. For example, Wang et al. (2013) prepared the trigonal Phase I (space group $P3_121$) at room temperature, the monoclinic Phase II ($P2_1/n$) by hydrothermal method at 180 °C, and the Phase III ($P2_1/m$) by heating to 750 °C. In nature, the formation of Phase III at lower temperatures can be expected due to the influence of unspecified factors such as chemical composition, pH and Eh of the circulating solutions.

Acknowledgements

The authors wish to express their thanks to Boris Ekrt (National Museum, Prague) for taking the SEM photos of zaïrite. The study was financially supported by the Ministry of Culture of the Czech Republic (long-term project DKRVO 2024-2028/1.II.a; National Museum, 00023272).

References

Achary SN, Errandonea D, Muñoz A, Rodríguez--Hernández P, Manjón FJ, Krishna PSR, Patwe SJ, Grover V, Tyagi AK (2013) Experimental and theoretical investigations on the polymorphism and metastability of $BiPO_4$. Dalton Trans 42: 14999-15015

Alves P, Viñals J, Rewitzer C, Vila F, Meisser N (2016) Folgosinho: Secondary phosphates from the Sitio do Castelo mine - Gouveia, Guarda, Portugal. Mineral Up 4: 6-27

Cepedal A, Martínez-Abad I, Fuertes-Fuente M, Lima A (2013) The presence of plumboan ingodite and a rare Bi-Pb tellurosulfide, $Pb_3Bi_4Te_4S_5$, in the Limarinho gold deposit, Northern Portugal. Can Mineral 51: 643-651

Di J, Chen J, Ji M, Zhang Q, Xu L, Xia J, Li H (2017) Reactable ionic liquid induced homogeneous carbon superdoping of $BiPO_4$ for superior photocatalytic removal of 4-chlorophenol. Chem Eng J 313: 1477-1485

Errandonea D, Gomis O, Santamaria-Perez D, García-Domene B, Muñoz A, Rodríguez-Hernández P, Achary SN, Tyagi AK, Popescu C (2015) Exploring the high-pressure behavior of the three known polymorphs of $BiPO_4$: Discovery of a new polymorph. J Appl Phys 117: 105902

Frost RL, Palmer SJ, Xi Y, Čejka J, Sejkora J, Plášil J (2013) Raman spectroscopic study of the hydroxy-phosphate mineral plumbogummite $PbAl_3(PO_4)_2(OH,H_2O)_6$. Spectrochim Acta A: Molecul Biomolecul Spectrosc 103: 431-434

Garate-Olabe I, Roda-Robles E, Gil-Crespo PL, Pérez A, Vieira R, Lima A (2012) Estudio textural y mineralógico del dique de cuarzo con fosfatos de Folgosinho (Guarda, Portugal). Macla 16: 220-221

Haq MR, Ehsan N, Nishat SS, Hossain QS, Khan MNI, Bashar MS, Akhtar US, Chowdhury F, Jahan S, Hossain KS, Khan MM, Imran SMS, Ahmed I (2024) Comprehensive first-principles modelling of experimentally synthesized $BiPO_4$ polymorphs. J Phys Chem C 128(11): 4779-4788

Jambor JL, Vanko DA (1991) New mineral names. Am Mineral 76: 1434-1440

Kampf AR, Grey IE, Alves P, Mills SJ, Nash BP, MacRae CM, Keck E (2017) Zincostrunzite, $Zn-Fe^{3+}_2(PO_4)_2(OH)_2{\cdot}6.5H_2O$, a new mineral from the Sítio do Castelo mine, Portugal, and the Hagendorf-Sud pegmatite, Germany. Eur J Mineral 29: 315-322

Lafuente B, Downs RT, Yang H, Stone N (2015) The power of databases: the RRUFF project. In: Armbruster T, Danisi RM, eds, Highlights in Mineralogical Crystallography, Berlin, Germany, W. De Gruyter: 1-30

Libowitzky E (1999) Correlation of O-H stretching frequencies and O-H···O hydrogen bond lengths in minerals. Monat Chem 130: 1047-1059

Mills SJ, Kampf AR, Raudsepp M, Birch W D (2010) The crystal structure of waylandite from Wheal Remfry, Cornwall, United Kingdom. Mineral Petrol 100: 249-253

Mindat (2024a) Ximegite: Mineral information, data and localities. Accessed on April, 2024 at https://www.mindat.org/min-4337.html

Mindat (2024b) Zaïrite: Mineral information, data and localities. Accessed on April, 2024 at https://www.mindat.org/min-4382.html

Monteles IA, Penha BV, Fonseca WS, Silva LMB, Santos ECS, de Souza LKC, Santos CC, de Menezes AS, Sharma SK, Javed Y, Khawar MR, Tanaka AA, Almeida MAP (2023) Bi-phasic $BiPO_4$ prepared through template-assisted hydrothermal method with enhanced electrochemical response for hybrid supercapacitor applications. J Appl Electrochem 53: 1609-1622

Naciri Y, Hsini A, Ajmal Z, Navío JA, Bakiz B, Albourine A, Ezahri M, Benlhachemi A (2020) Recent progress on the enhancement of photocatalytic properties of $BiPO_4$ using π-conjugated materials. Adv Colloid Interface Sci 280: 102160

Nakamoto K (2009) Infrared and Raman spectra of inorganic and coordination compounds Part A Theory and applications in inorganic chemistry. John Wiley and Sons Inc. Hoboken, New Jersey

Pan C, Zhu Y (2015) A review of $BiPO_4$, a highly efficient oxyacid-type photocatalyst, used for environmental applications. Catal Sci Technol 5: 3071-3083

Pechkovski VV, Melnikova PY, Dzyubova ED, Barannikova MV, Nikanovich M (1981) Atlas of Infrared Spectra of Phosphates. Orthophosphates. Nauka Moscow (in Russian)

Pouchou JL, Pichoir F (1985) "PAP" (φρZ) procedure for improved quantitative microanalysis. In: Microbeam Analysis (J. T. Armstrong, ed.). San Francisco Press, San Francisco: 104-106

Sejkora J, Dolníček Z, Plášil J (2023) Ammoniozippeite from the Jáchymov ore district, Krušné hory Mountains (Czech Republic) - description and Raman spectroscopy. Bull Mineral Petrolog 31(1): 1-9

Shi J (1989a) Ximengite - a new mineral. Acta Mineral Sin 63: 15-19 (in Chinese). Cited in Jambor, Vanko (1991)

Shi J (1989b) A new mineral - Ximengite. Chin J Geochem 8(4): 385-391

Tvrdý J, Sejkora J, Rosseel P, Dolníček Z (2021) Ferraioloite from the Sítio do Castelo mine, Folgosinho (Guarda, Portugal), description and Raman spectroscopy. J Geosci 66(3): 139-146

Van Wambeke L (1975) La zaïrite, un nouveau minéral appartenant à la série de la crandallite. Bull Minéral 98: 351-353

Wang YJ, Li LP, Zheng J, Huang XS, Li GS (2013) Synthesis, photoluminescence and photocatalytic performance of $BiPO_4$ with different phase structures. Chem Res Chin Univ 29(3): 556-562